PHYSICAL CONDITIONS AND KINEMATICS OF THE FILAMENTARY STRUCTURE IN ORION MOLECULAR CLOUD 1

Yu-Hsuan Teng (UCSD) and Naomi Hirano (ASIAA)

It is known that filamentary structures are prevalent in star-forming clouds and are believed to play an important role in star formation processes (e.g. Schneider & Elmegreen 1979; Andre et al. 2014). The sizes of filaments in star-forming regions range from parsec to subparsec scales, and a large-scale filament may consist of narrower filaments at a smaller scale. For example, the northern part of the Orion A molecular cloud, which is the nearest high-mass star-forming region at a distance of 414 pc (Menten et al. 2007), is an integral-shape filament with >13 pc long and ~0.5 pc wide (Bally et al. 1987). Residing at the center of the integral-shape filament, the Orion Molecular Cloud1 (OMC1) is the most massive component (>2200 $M_{\odot}$) and the most active star-forming region in the cloud (Bally et al. 1987). Previous interferometric observations of NH_3 with the Very Large Array (VLA) (Wiseman & Ho, 1998) and N_2H^+ 1–0 with the Atacama Large Millimeter/submillimeter Array (ALMA) (Hacar et al. 2018) revealed that OMC1 consists of smaller-scale filaments of high density gas. The dense cores inside these small-scale filaments could be current or future sites for star formation.

Using the Submillimeter Array (SMA), we have observed the N_2H^+ 3–2 emission from OMC1 at an angular resolution of ~5.4'' (~2300 au). Our 144-pointing mosaic observations covering the 6' × 9' (0.7 pc × 1.1 pc) area of OMC1 were combined with the single-dish data obtained with the Submillimeter Telescope (SMT) in order to recover the spatially extended emission. Figure 1 shows the combined moment 0 (integrated intensity) and moment 1 (intensity-weighted radial velocity) maps. The moment 0 map clearly shows that most of the

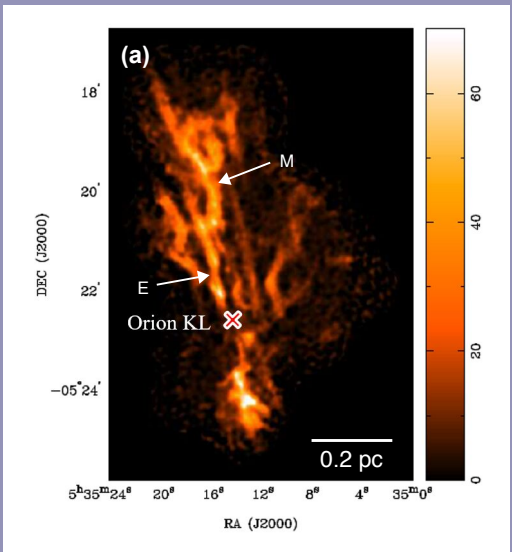

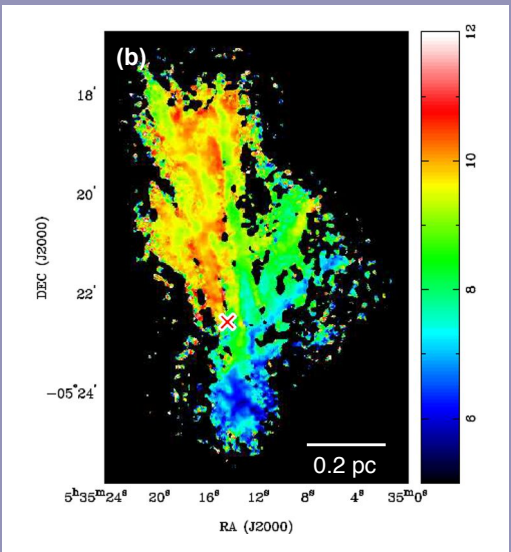

Figure 1a (left) **and 1b** (right): Moment 0 (K km s^{-1}) and moment 1 (km s^{-1}) maps of the combined SMA and SMT data in N_2H^+ 3–2. The cross depicts the position of Orion KL at (R.A., decl.) = (5^h 35^m $14^s.5$, -5°22'30''). The arrows indicate the two prominent filaments with core fragmentation.

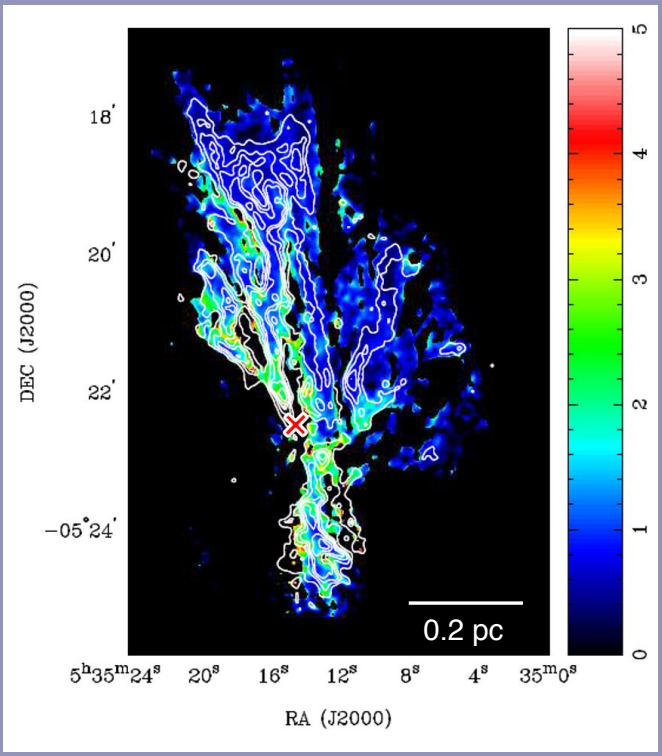

Figure 2: N_2H^+ 3–2/1–0 intensity ratio map using 1–0 image observed with ALMA + IRAM 30m (Hacar et al. 2018). Contour levels of N_2H^+ 3–2 moment 0 are overlaid on the line ratio map. The cross marks the position of Orion KL.

emission comes from the filamentary structure with a typical width of 0.02–0.03 pc. Several high-intensity and clumpy structures can also be seen inside the filaments. By applying *FilFinder* (Kock & Rosolowsky, 2015) and *2D Clumpfind* (Williams et al. 1994) on the combined image, we identified 11 filaments and 10 cores, respectively.

As revealed in Figure 1b, the OMC1 region consists of three subregions having different radial velocities with sharp velocity transitions. The northern region, with bright filaments to the north of Orion KL, has a velocity range of ~9–11 km s^{-1}; the western region, with fainter filaments extending to the northwest, is observed at ~7–9 km s^{-1}; and the southern region, also known as OMC1-South, is at ~5–7 km s^{-1}. These three subregions with different velocities converge at the Orion KL region. Such velocity structure of OMC1 can be interpreted as large-scale inflowing gas being accelerated toward the Orion Nebula Cluster (Peretto et al. 2013; Hacar et al. 2017). The morphology of magnetic fields in OMC1 observed by the JCMT BISTRO Survey (Pattle et al. 2017) also supports this global collapse scenario.

To analyze the physical conditions of the dense gas, we made the 3–2/1–0 ratio map (Figure 2) using our SMA + SMT data and the ALMA + IRAM 30 m data provided by Hacar et al. (2018). Using the non-LTE radiative transfer code RADEX (van der Tak et al. 2007), we modeled the integrated intensities of N_2H^+ 3–2 and 1–0 and the 3–2/1–0 intensity ratios under various combinations of H_2 density (n_{H2}), kinetic temperature (T_{kin}), and the ratio of N_2H^+ column density to line width ($N(N_2H^+)/\Delta v$).

The N_2H^+ 3–2/1–0 ratio map presented in Figure 2 reveals higher ratios overall in the eastern part of OMC1. In addition, the 3–2/1–0 ratio tends to be lower in the filament regions (1 ± 0.3) as compared to the surrounding nonfilament regions (2.2 ± 0.4). The non-LTE models have revealed that the filament regions have a higher density of ~10^7 cm^{-3} and a lower temperature of ~15–20 K than the nonfilament regions. Inside the filaments, the volume density of the core regions (1–3 × 10^7 cm^{-3}) are generally higher than the lower intensity regions (3–10 × 10^6 cm^{-3}), while there is no significant difference in temperature between the core and the lower intensity regions. Using the volume densities determined from the non-LTE analysis, we have estimated the masses of the cores and the line masses of the filaments. The masses of the cores are in the range of 1–10 $M_\odot$, which are similar to their virial masses. We also found that 7 of the 11 identified filaments have line masses between 0.5 to 1.5 times their critical line masses. These results indicate that most of the OMC1 filaments and cores are gravitationally bound.

The higher 3–2/1–0 ratio in the eastern part of OMC1 suggests that the eastern OMC1 has higher temperatures compared with the remaining area. The overall distribution of the high-ratio gas in eastern OMC1 is similar to that of the CN and C_2H molecules, which are both sensitive to the presence of UV radiation (Ungerechtset al. 1997; Melnick et al. 2011). Therefore, the higher temperatures in the eastern OMC1 could be due to external UV heating from the high-mass stars in M42 (e.g. θ^1Ori C) and M43 (e.g. NU Ori). In addition, it is likely that the dense gas in the filaments could block the external radiation, which may explain why the filament regions have high densities and lower temperatures.

We also investigated the gas kinematics inside the two prominent filaments with core fragmentation (labeled 'E' and 'M' in Figure 1a). We found that one of the filaments (E) shows interesting oscillation patterns along its major axis in both intensity and velocity fields (Figure 3). The intensity and velocity peaks toward two of the cores reveal positional shifts of ~λ/4, which is indicative of inflowing gas motions toward these cores (Hacar & Tafalla 2011). Therefore, it is possible that core formation is still ongoing in this filament. On the other hand, similar features were not observed in the other filament (M), where evidences of young protostars have been reported (e.g. Teixeira et al. 2016). It is thus likely that filament

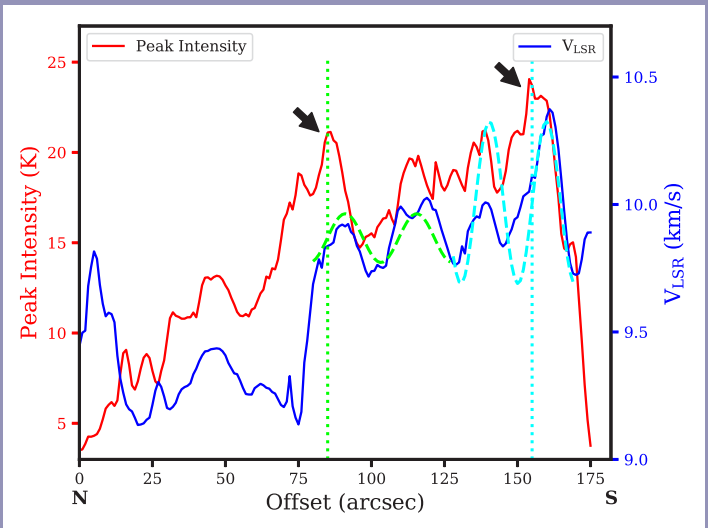

Figure 3: Intensity and velocity variations along the major axis of filament E labeled in **Figure 1a.** The arrows indicate two intensity peaks showing positional shifts relative to their velocity peaks; the dashed curves are sinusoidal fits to the velocity variation, and the two vertical lines show the locations shifted by λ/4 from the fitted sinusoidal peaks of the two cores. Offset 0 is at the northernmost position of this filament.

E is in an earlier evolutionary phase than filament M with star formation signature.

In conclusion, our high-resolution N_2H^+ 3–2 image obtained by combining the SMA and SMT data reveals that OMC1 is a bundle of dense gas filaments. Dense gas in this region is collapsing globally toward the high-mass star-forming region, Orion Nebula Cluster. The eastern part of OMC1 is heated externally from high-mass stars in M42 and M43. Nevertheless, the gas in the filaments remains cold thanks to the shielding from the external heating due to high density. The signature of core-forming gas motions, which is similar to that found in low-mass star-forming regions, is also found in one of the filaments with core fragmentation. Further details of this work are presented in Teng & Hirano (2020).

REFERENCES

- André, P., Di Francesco, J., Ward-Thompson, D., et al. 2014, in Protostars and Planets VI, ed. H. Beuther et al. (Tucson, AZ: Univ. Arizona Press), 27
- Bally, J., Langer, W. D., Stark, A. A., & Wilson, R. W. 1987, ApJ, 312, L45
- Hacar, A., Alves, J., Tafalla, M., & Goicoechea J. R. 2017, A&A, 602, L2
- Hacar, A., & Tafalla, M. 2011, A&A, 533, A34
- Hacar, A., Tafalla, M., Forbrich, J., et al. 2018, A&A, 610, A77
- Koch, E. W., & Rosolowsky, E. W. 2015, MNRAS, 452, 3435
- Melnick, G. J., Tolls, V., Snell, R. L. et al. 2011, ApJ, 727, 13
- Menten, K. M., Reid, M. J., Forbrich, J., & Brunthaler, A. 2007, A&A, 474, 515
- Pattle, K., Ward-Thompson, D., Berry, D. et al. 2017, ApJ, 846, 122
- Peretto, N., Fuller, G. A., Duarte-Cabral, A., et al. 2013, A&A, 555, A112
- Schneider, S. & Elmegreen, B. G. 1979, ApJS, 41, 87
- Teixeira, P. S., Takahashi, S., Zapata, L. A. & Ho, P. T. P., 2016, A&A, 587, A47
- Teng, Y.-H., & Hirano, N. 2020, ApJ, 893, 63
- Ungerechts, H., Bergin, E. A., Goldsmith, P. F. et al. 1997, ApJ, 482, 245
- Van der Tak, F. F. S., Black, J. H., Schoier, F. L., et al. 2007, A&A, 468, 627
- Williams, J. P., de Geus, E. J., & Blitz, L. 1994, ApJ, 428, 693
- Wiseman, J., & Ho, P. T. P. 1998, ApJ, 502, 676